J. Inst. Eng. India Ser. C (June 2020) 101(3):441–450
https://doi.org/10.1007/s40032-020-00565-8

ORIGINAL CONTRIBUTION

Study on Influence of Environmental Parameters on Dynamic Stall Characteristics of Wind Turbine Blades

Long Wang[1] · Cheng Wang[1] · Lunye Sun[1]

Received: 13 July 2019 / Accepted: 11 January 2020 / Published online: 20 January 2020
© The Institution of Engineers (India) 2020

Abstract Wind turbines in complex environments could encounter dynamic loads that deviate from design values, while the dynamic stall problem could reduce the reliability and safety of wind turbines. In order to accurately evaluate the aerodynamic characteristics of wind turbine blades, the influence on the dynamic stall characteristics of wind turbine airfoil under complex wind farm environmental factors is studied. The variation law of lift coefficient under different working conditions is obtained, and the pressure coefficient and flow field distribution with times are given. The evolution characteristics of vortex on airfoil surface are analyzed. The results show that when the unsteady effect is significant, the closed-loop area of the blades lift coefficient is gradually larger, and the angle of attack for the maximum lift is proportional to it; when the oscillation angle becomes larger, the upper and lower extreme values of the lift force increase, and the lift curve is more obvious in the shape of the oblique "∞." When the blade appears to be in dynamic stall, the lift coefficient increases quickly and has a hysteresis effect. The maximum increase is up to 46.15%, and the hysteresis effect occurs. The instability of the shear layer, the formation and quenching of the trailing edge vortex are the main causes of the hysteresis effect for the blade lift coefficient. Reasonable evaluation of its value is of great significance for wind turbine blade design in complex wind farm environment.

✉ Lunye Sun
2879391552@qq.com

[1] School of Mechanical Engineering, Anhui University of Science and Technology, Huainan 232001, China

Keywords Computational fluid dynamics · Wind turbine airfoil · Dynamic stall · Flow separation · Unsteady effect

Introduction

With the vigorous development of economies and industries in the world, the contradiction between the energy demand and the exhaustion of traditional energy sources has become increasingly prominent; however, wind energy has a huge advance prospect as an environmentally friendly and pollution-free green renewable energy source [1]. As a carrier for capturing wind energy, wind turbines have caught the attention of scholars all over the world. However, the complex environment of wind farms will cause the problems such as dynamic stall of wind turbines, restricting the promotion of wind turbine blades, which is not conducive to the use of renewable energy [2, 3]. Dynamic stall is a phenomenon often seen in the operation of wind turbine blades, and its aerodynamic coefficient is quite different from the static stalls, which exhibits periodic fluctuations [4]. Once the unsteady aerodynamic load acts on the wind turbine blade for a long time, it will cause fatigue and damage to the wind turbine structure. Finally, the actual service life of the wind turbine is much lower than the design life.

At first, the dynamic stall phenomenon appeared on the helicopter rotor. The dynamic stall experiment of the aviation airfoil is performed by McCroskey et al. [5], and the variation law involving the lift and drag coefficient of the aeronautical airfoil is compared and analyzed. In recent years, the wind turbine blades have been correspondingly researched at home and abroad. The S809 airfoil extensively is applied today as a wind turbine airfoil. So the

National Renewable Energy Laboratory (NREL) has conducted several groups of wind tunnel experiments to it based on the strict requirements of incoming conditions, and relatively accurate experimental data have been obtained. The experimental results can be used as evaluation criteria for different numerical calculation methods [6]. The effect of slitting on the lift of wind turbines has been studied by Long et al. [7, 8], and the results show that the slitting can be used as an effective means to improve the lift of the airfoil.

Gerontakos studies the effect of flapping motion on the oscillating NACA 0012 airfoil. The flap motion can change the starting position of the vortex structure and has a greater influence on both the lift and drag [9]. On this basis, the impact on the airfoil wake under the condition that the leading edge cylinder rotated is studied by Gerontakos et al. [10] using particle image velocimetry. It is noted that the separation of the boundary layer is delayed and the width of the wake vortex structure was reduced.

Yang et al. [11] also select the S809 airfoil as the research object and describe the vortex structure progress of the airfoil flow field. Kim Y uses the large eddy simulation method for studying the aerodynamic characteristics of the pitch airfoil. The calculated average lift, drag and torque of the airfoil agree well with the experimental data [12]. Yen et al. [13] adopt synthetic jet control to improve the dynamic stall effect of low-speed blades, which could enhance the safety of wind turbines. A dynamic stall model for S809 is established by Gupta, and its effectiveness is checked by experiments [14]. Pengyin et al. study the reduction model of dynamic stall for wind turbines. Considering its computational cost and relatively low consumption resources, it is useful to analyze and optimize the aeroelastic problem of wind turbines [15]. Mao carries out an experimental study on the separation flow of the airfoil which pitches up at the constant velocity and qualitatively explains the reason for the high lift of the airfoil [16]. Peng et al. numerically simulate the dynamic stall process of the airfoil which pitches up at the constant velocity. Increasing the upward rate can delay the stall and improve the flow field and increase the airfoil output power [17].

The above research on dynamic stall mainly focuses on low wind speed conditions of aeronautical airfoil or wind turbine airfoil, while rarely does the study on the dynamic stall characteristics of wind turbine airfoil in high wind speed environment reported. Considering the wide application prospects of offshore wind turbines, this paper takes the S809 airfoil as the research object [18, 19] and uses computational fluid dynamics to study the influence of environmental parameters on the dynamic stall of wind turbine airfoils under high wind speed conditions. The variation of lift coefficient and the evolutionary characteristics of the flow field structure are obtained, and the dynamic stall mechanism of airfoil under high wind speed is clarified. The research is beneficial to the design and manufacture of offshore wind turbine blades.

Numerical Simulation Theory

Control Equations and Turbulence Models

The *N–S* equation of fluid in Cartesian coordinate system [18–20] is as follows:

$$\frac{\partial}{\partial t}\iiint_{\Omega} Q\mathrm{d}V + \oiint_{\partial\Omega}(F(Q) - G(Q))\cdot n\mathrm{d}S = 0 \tag{1}$$

where Ω is control body, $\partial\Omega$ is the corresponding boundary, Q is a conservation variable, $F(Q)$ is the inviscid flux, $G(Q)$ is the viscous flux, and n is the external normal vector of control body. The detailed meaning of expression can be found in the literature [20–22].

$$Q = \begin{bmatrix} \rho \\ \rho u \\ \rho v \\ \mathrm{e} \end{bmatrix},\quad F(Q)\cdot n = (V\cdot n)\begin{Bmatrix} \rho \\ \rho u \\ \rho v \\ e+p \end{Bmatrix} + p\begin{Bmatrix} 0 \\ n_{\mathrm{x}} \\ n_{\mathrm{y}} \\ 0 \end{Bmatrix},$$

$$G(Q)\cdot n = \frac{M_{\infty}}{\mathrm{Re}}\left(n_{\mathrm{x}}G_1 + n_{\mathrm{y}}G_2\right),$$

$$G_1 = \begin{Bmatrix} 0 \\ \tau_{\mathrm{xx}} \\ \tau_{\mathrm{yx}} \\ u\tau_{\mathrm{xx}} + v\tau_{\mathrm{yx}} - \hat{q}_{\mathrm{x}} \end{Bmatrix},\quad G_2 = \begin{Bmatrix} 0 \\ \tau_{\mathrm{xy}} \\ \tau_{\mathrm{yy}} \\ u\tau_{\mathrm{xy}} + v\tau_{\mathrm{yy}} - \hat{q}_{\mathrm{y}} \end{Bmatrix} \tag{2}$$

The turbulence model selected in this paper is the Spalart–Allmaras (S–A) model [23–25], and the formula is as follows:

$$\frac{\partial}{\partial t}(\rho\tilde{v}) + \frac{\partial}{\partial x_i}(\rho\tilde{v}u_i) = G_v + \frac{1}{\sigma\tilde{v}}\left\{\frac{\partial}{\partial x_j}\left[(\mu+\rho\tilde{v})\frac{\partial\tilde{v}}{\partial x_j}\right] + G_{b2}\rho\left(\frac{\partial\tilde{v}}{\partial x_j}\right)^2\right\} - Y_v + S_{\tilde{v}} \tag{3}$$

The meanings of the above formulas can be discovered in the literature [23]. To some extent, the S–A turbulence model can solve the turbulence problem. It is a turbulence model that is more applicable to airfoil aerodynamic calculations, with capturing the characteristics of flow separation [23].

Numerical Simulation Parameters

The S809 airfoil commonly used in horizontal axis wind turbines is selected as the research object. The environmental parameters are replaced by three characteristic quantities, namely wind speed, angle of attack and reduced frequency. Wherein the angle of attack can represent the flow direction of natural wind relative to the airfoil, and the reduced frequency represents the unsteady characteristic of natural wind.

Assuming that the airfoil makes a sinusoidal oscillation motion about the 1/4 position of the chord length, the angle changes during the movement as follows:

$$\alpha(t) = \alpha_0 + \alpha_1 \sin(2\pi f t) \tag{4}$$

In the formula, α_0 means angle of attack, and α_1 represents oscillation amplitude. Respectively, f is oscillation frequency and t means time.

The reduced frequency is an important aerodynamic parameter describing the unsteady level of the oscillating airfoil [14], and its formula is defined as follows:

$$k = \omega c/2u_\infty = \pi f c/u_\infty \tag{5}$$

Flow classifications characterized by different reduced frequencies will be different. (1) When the reduced frequency is 0, the flow is considered to be a constant flow. (2) When the reduced frequency is greater than 0 and less than 0.5, the flow field is close to steady flow. The unsteady effect has less effect on the flow field, and it can be completely ignored in some special cases. (3) Once the reduced frequency is greater than 0.5, the flow field is unsteady, and if the value exceeds 0.2, the flow is in a highly unsteady state.

Meshing

The dynamic stall of airfoil was analyzed by combining dynamic grid technique [26–28] and CFD method [29–31]. Figure 1 shows the grid of airfoil, with the grid of the airfoil computational domain and the partially enlarge grid around the airfoil. The robustness of dynamic mesh is crucial to the calculation, so the triangle grid with better stability is selected. The number of the grid is about 30,000. Figure 1a shows the whole computing domain. For better capturing the details of flow field structure, there is a local encryption near the blade region. Figure 1b shows the result that this grid setting can guarantee the stability of calculation, and the boundary condition of computational domain is set to the far field condition. The calculated results of each working condition in this paper are calculated through multiple cycles. After the periodic stable changes in lift force are observed, the data of the last cycle are selected for analysis and processing.

Results and Analysis

Test Verification

The aerodynamic parameters used in the verified example are the same as experimental conditions of the OSU in the USA [32]. Parameters are as follows: Reynolds number Re = 10^6, reduced frequency k = 0.050, initial attack angle $\alpha_0 = 8°$, amplitude of oscillation angle $\alpha_0 = 10°$. The work is done in ANSYS Fluent.

Figure 2a shows the curve of lift force changing with angle of attack for the airfoil. The trends between CFD simulation data and OSU experimental data are generally the same, and the lift coefficient is consistent with the experimental values. After the angle of attack is more than 8°, the difference between the calculated data and experimental data slightly increases. The reason derives from the

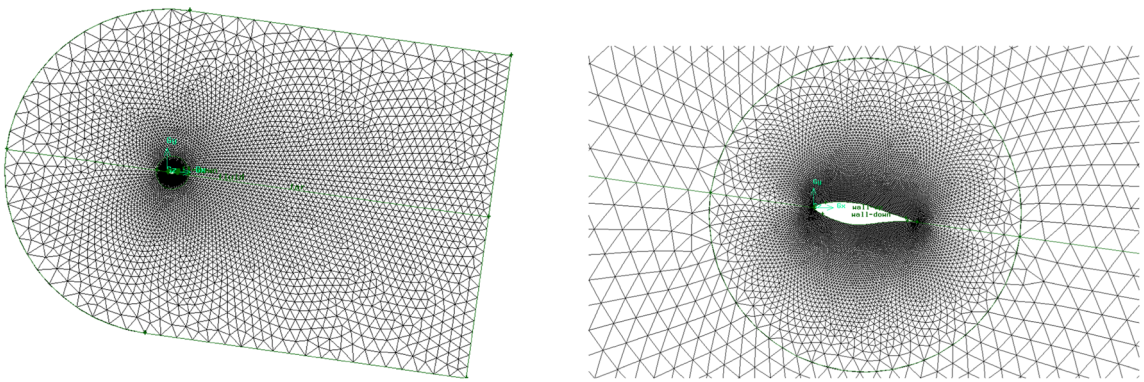

(a) Airfoil computing domain **(b)** Surrounding grid of airfoil

Fig. 1 The grid of S809 airfoil

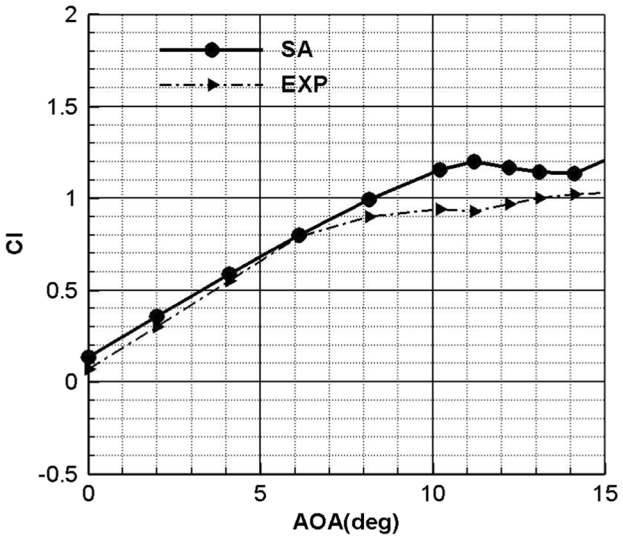

(a) Static contrast data

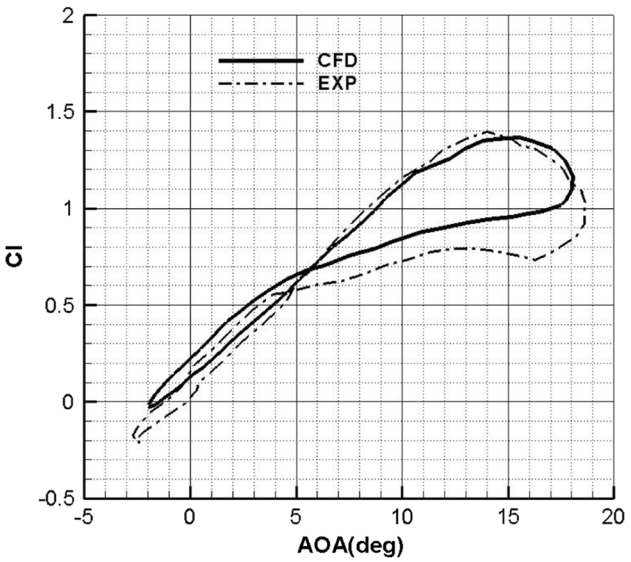

(b) Dynamic contrast data

Fig. 2 The comparison of experiment and calculation

turbulence model for the accuracy of flow separation phenomenon and the flow resistance simulation. It has a good consistency between the OSU experimental values, and the aerodynamic hysteresis closed curve computed by S–A turbulence model and two hysteresis closed curves have the same tendency.

The lift coefficient is equal to the OSU experimental value in the process of pitch up, but the CFD simulated data have a slight difference with experimental data in the process of pitch down. The reason is the same as the static calculation, which is also one of the challenges in computational fluid dynamic. By comparing Fig. 2, the lift coefficient can increase 40% higher than the original data in the case of dynamic stall. This effect must be considered when designing the structure of wind turbine blades; otherwise, it has a harmful influence on the life of blades.

The CFD method has good agreement on experimental data from the OSU for simulating the static and dynamic stall of airfoil. Although there is a numerical deviation at some state points, it has little effect on the research on the aerodynamic characteristics of airfoils. Finally, it is feasible that CFD method is used to study the dynamic stall characteristics of airfoils at high wind speed.

Hysteresis Characteristics of Lift Coefficient Curve

In the actual operation of offshore wind turbines, most of wind turbine blades may crack and damage after servicing a period due to the dynamic stall phenomenon at high wind velocity. At high wind velocity, the dynamic stall characteristics are studied by choosing different oscillation angles and reduced frequency at the extreme wind velocities (40 m/s and 50 m/s) in the paper.

Figures 3 and 4 show that the velocity of 40 m/s and 50 m/s, initial angle of attack of 12^0, when the oscillation angles are 5^0, 10^0 and 15^0, and the reduced frequency is 0.026, 0.050 and 0.075. There are 18 operating conditions with the variations of the lift coefficient in total. In order to distinguish different working conditions, digital notation was selected for marking. For example, "40-12-5-0.026" shows the incoming wind velocity of 40 m/s, the initial angle of attack of 12^0, the oscillation angle of attack of 5^0, and the reduced frequency of 0.026.

With comparing the three hysteresis curves of lift coefficient in Fig. 3a–i, when the other parameters remain unchanged, with the increase in the reduced frequency, the area surrounded by the hysteresis curve of lift coefficient magnifies and the distribution curve of lift coefficient broadens. With the decrease in the reduced frequency, the area surrounded by the hysteresis curve of lift coefficient reduces and the distribution curve of lift coefficient narrows.

In the case of the larger reduced frequency, because the aerodynamic alternating load changes greatly corresponding to the larger amplitude of alternating stress, it is a challenge to the bearing capacity of the blade. So the structure design of the blade has to be considered to the effect on dynamic stall.

The stall angle of attack with the lift coefficient peak increases with the larger of reduced frequency, and this phenomenon becomes more obvious with the angle of attack of oscillation increasing.

In addition, the reduced frequency has an effect on the intersection angle of the lift curve. The change in the intersection angle is opposite to the transformation of reduced frequency. The larger the reduced frequency is, the smaller the intersection angle is.

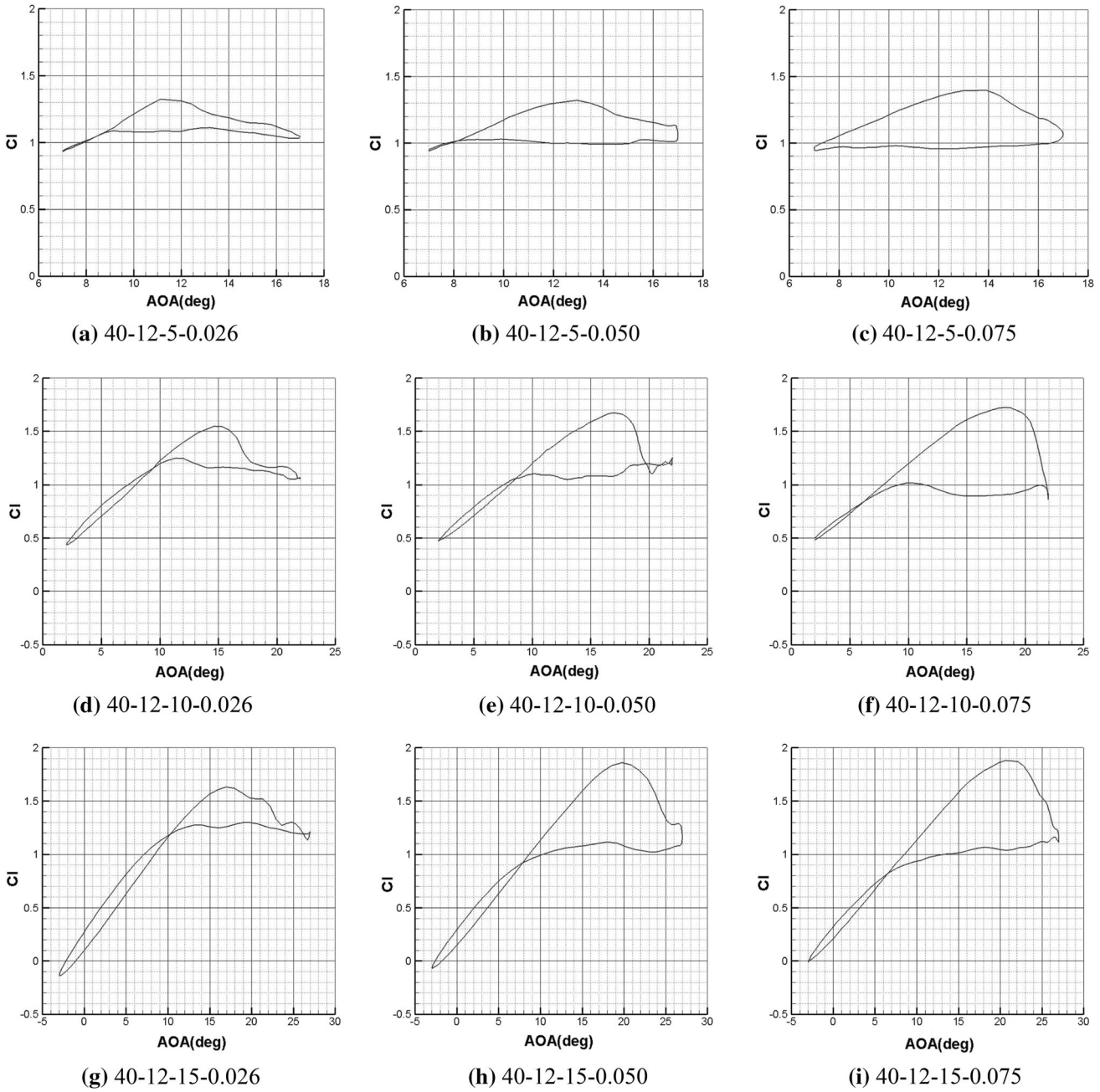

Fig. 3 The chart of lift coefficient with different parameters under 40 m/s wind

In Fig. 3a, the maximum lift coefficient is 1.3, but the maximum lift coefficient in Fig. 3i could be 1.9, whose growth is about 46.15%. It can be seen that the oscillation angle and reduced frequency have great influence on the lift coefficient, and thereby the working performance of wind turbine blade is affected.

The lift coefficient is staggered with local oscillation in Fig. 3e, g, because of the large scale vortex structure decomposing into small scale vortex shedding from the blade and change the area affected by vortex. There may be stall flutter problems, which should be avoided in wind turbine blade design.

Figure 4 shows the results of calculations under the 50 m/s condition, and it can be found that the lift coefficient of the wind turbine blade at the ultimate wind velocity is slightly larger than the one under the 40 m/s condition, where the lift coefficient fluctuation is more obviously within the scale of a large angle of attack. It has no alternating phenomenon of lift coefficient under the whole working conditions, and the other laws are similar to 40 m/s.

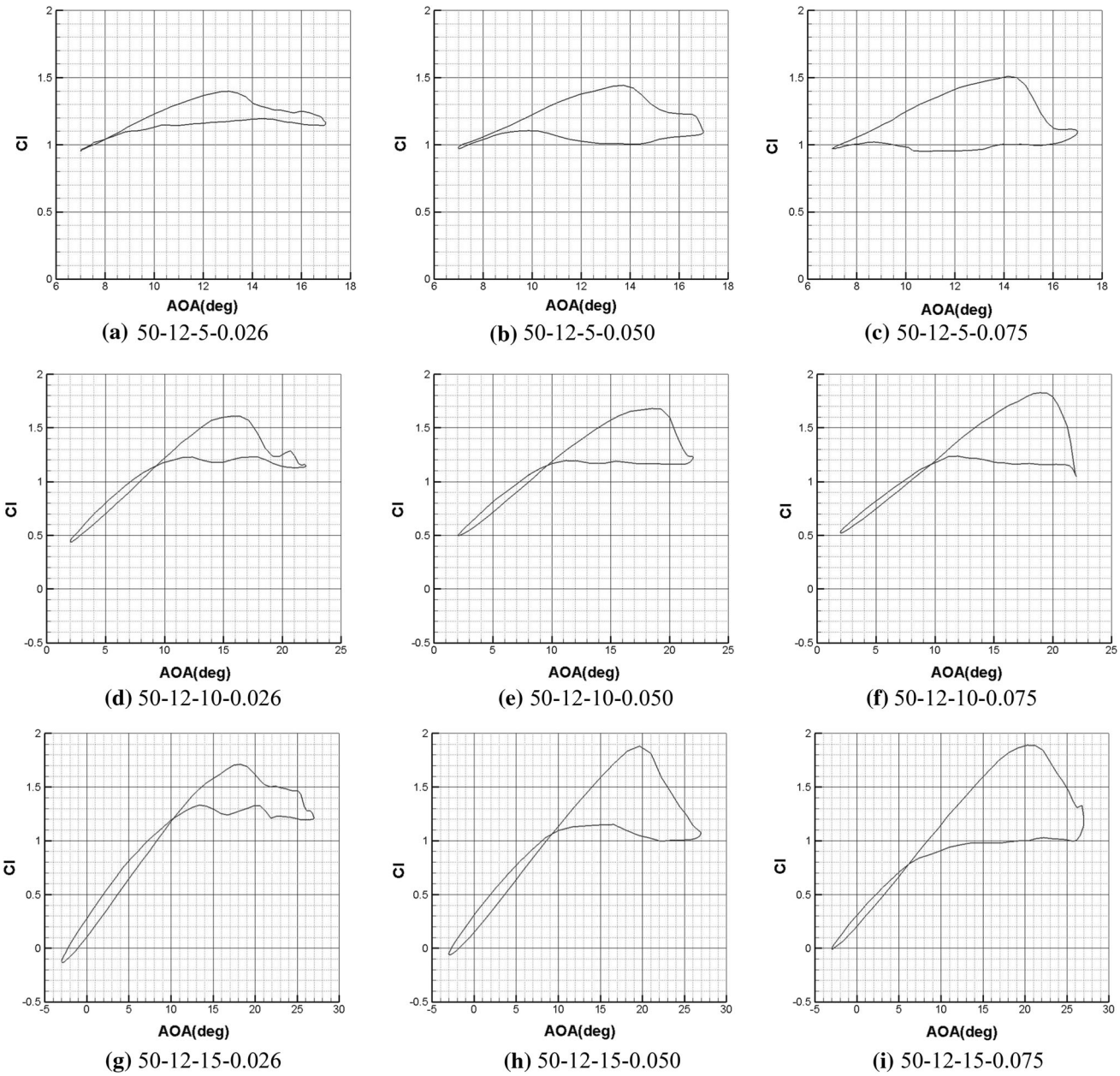

Fig. 4 The chart of lift coefficient with different parameters under 40 m/s wind

Analysis of Flow Field

For dynamic stall at high wind speeds, a wind speed of 40 m/s can cause the airfoil to fall into deep stalls. Once the wind turbine is in a deep stall state for a long time, this is easy to cause blade breakage and other damage. Therefore, the flow field of dynamic stall under the condition of 40 m/s is analyzed emphatically. The operating parameters selected are as follows: initial attack angle $\alpha_0 = 12^\circ$, oscillation angle $\alpha_1 = 10^\circ$, and the reduced frequency $k = 0.050$.

It shows the pressure coefficient distribution and corresponding flow field structure of the airfoil during pickup process in Fig. 5. Before no more than 14.82^0, the fluid adheres to the surface of the airfoil. There is no flow separation in the entire boundary layer around the airfoil, and the lift continues to increase, which causes that the stall attack angle is large and exceeds the static stall angle of attack. When the angle of attack increases to about 17^0, the airfoil begins to have a trailing edge vortex. As the angle of attack becomes larger, its influence area gradually increases and slowly extends toward the leading edge of the airfoil. The lift coefficient of the airfoil in dynamic stall reaches the maximum, and this conclusion could be obtained by observing the corresponding area of pressure coefficient distribution.

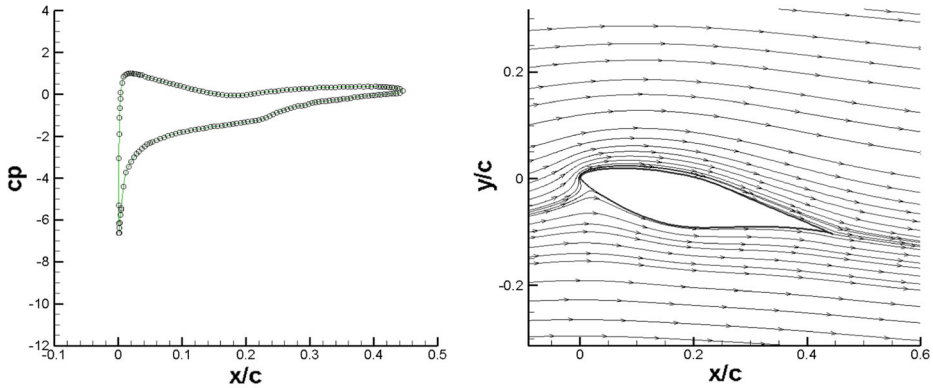

(a) Cl=1.57，α=14.82°

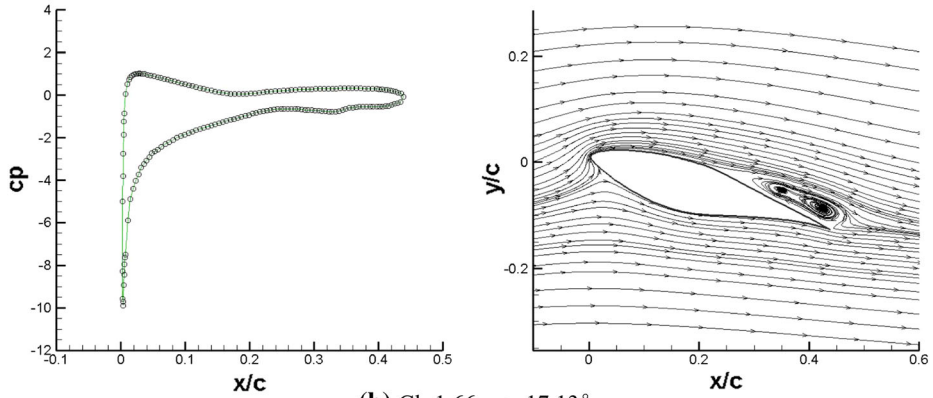

(b) Cl=1.66，α=17.13°

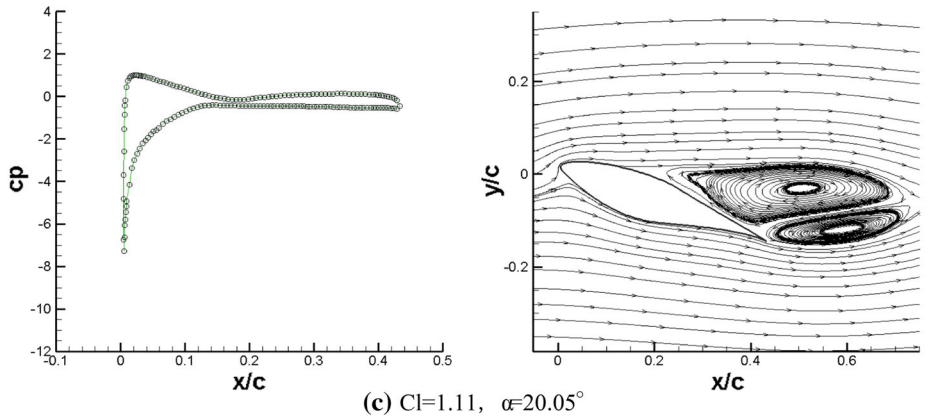

(c) Cl=1.11，α=20.05°

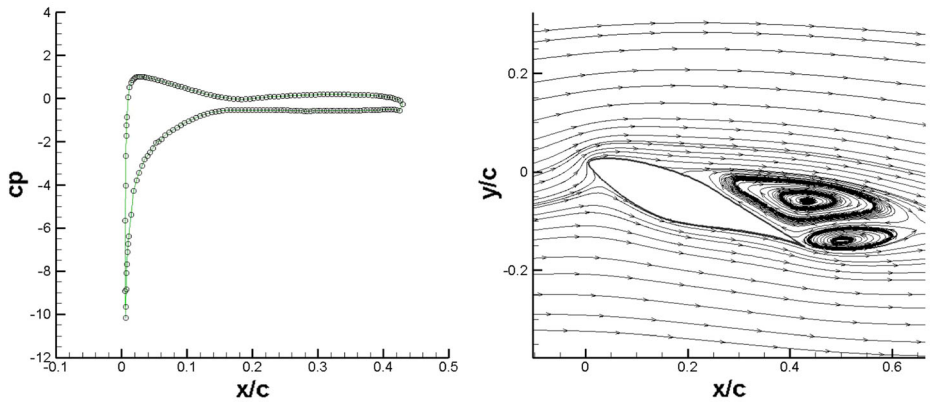

(d) Cl=1.18，α=21.75°

Fig. 5 The pickup streamline and surface pressure coefficient of S809 airfoil for u = 40 m/s, $\alpha_0 = 12°$, $\alpha_1 = 10°$, $k = 0.05$

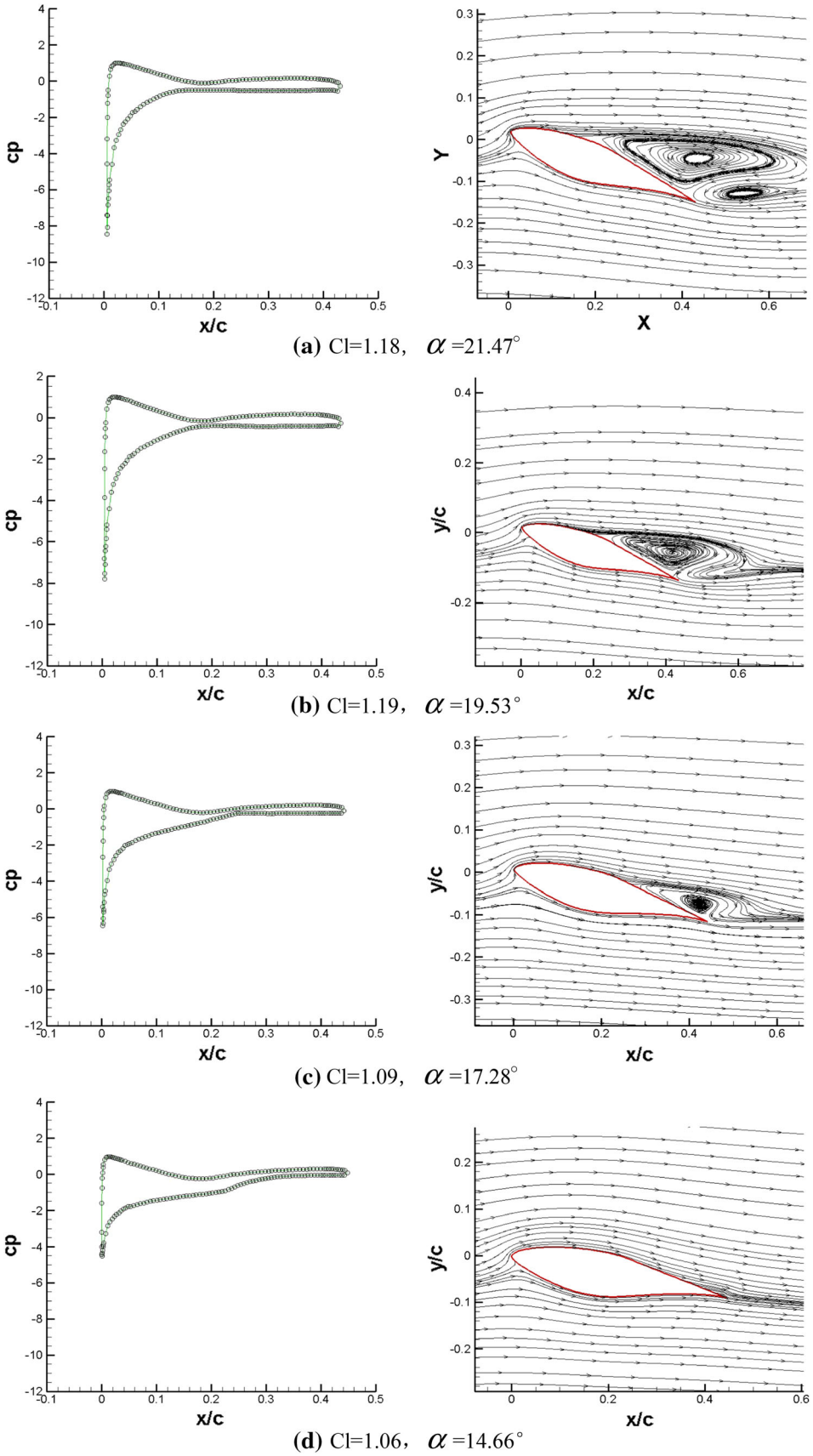

(a) Cl=1.18, α =21.47°

(b) Cl=1.19, α =19.53°

(c) Cl=1.09, α =17.28°

(d) Cl=1.06, α =14.66°

Fig. 6 The downward streamline and surface pressure coefficient of S809 airfoil for u = 40 m/s, $\alpha_0 = 12°$, $\alpha_1 = 10°$, $k = 0.05$

The vortex breaks into a double vortex when it increases to a certain extent, and its influence area will be larger. The back vortex would fall off from the trailing edge, and the separation point continues to approach the leading edge. The vortex structure can reach a region of 0.5 times chord length. The rolling of the fluid shear layer causes the vortex to expand and exhibit instability. The rupture and shedding motion of the vortex is the reason for the fluctuation of the lift. It could be seen that at the 20° angle of attack, the lift coefficient drops from the peak of 1.66–1.11. As the vortex intensity decays, the lift coefficient rises slightly at the 21.75^0 angle of attack.

Figure 6 shows the pressure coefficient distribution of surface and the corresponding flow field structure during the airfoil's downward motion. The vortex at the trailing edge of the airfoil becomes smaller and falls off the trailing edge. The lift coefficient is stable at about 1.18 and then slightly rises to 1.19. In the subsequent down motion, a change in flow separation requires a delay time to return to the previous attached flow state. After the airfoil is down to the 14.66^0 angle of attack, the vortex on the suction surface of the airfoil completely disappears, and the flow at this time is completely attached.

But the lift coefficient is completely different from the upward phase, which is also the characteristic of dynamic stall. Two different lift values correspond to the same angle of attack, and the hysteresis effect is very obvious. Comparing Figs. 5 and 6, the vortex structure directly affects the distribution pressure coefficient of the airfoil suction, thus changing the blade lift coefficient.

It can be found through the analysis above that flow separation is more serious under the high wind velocity, and the stall angle of attack is larger when the maximum lift of the airfoil is present. Meanwhile, it is greatly obvious that the vortex generates on the airfoil surface, ruptures and detaches from the airfoil. This effect on the lift coefficient which increases extremely is great. Also the effect of lift hysteresis is very clear.

Conclusion

The S809 airfoil with sinusoidal oscillation is simulated and analyzed based on the CFD numerical simulation method. It mainly studies the influence of three environmental parameters of wind speed, oscillation angle of attack and reduced frequency on the dynamic stall characteristics of wind turbines under the high wind speed condition. The work could provide guidance for the design and maintenance of wind turbine blades. The following conclusions are obtained.

1. Firstly, the CFD method is used to simulate the S809 airfoil, and the simulation results are compared with the OSU experimental data. The two lift curves are close, and there is little difference between the two data only at the large angle of attack. The reason is that the turbulence model has some errors in describing the phenomenon of flow separation, but the CFD method is feasible for dynamic stall simulation.
2. The influence of the two parameters which include oscillation angle and reduced frequency on lift is studied under the conditions of 40 m/s and 50 m/s. As the reduced frequency increases, the hysteresis closed area of the airfoil lift coefficient gradually increases, and the angle of attack corresponding to the maximum lift is proportional to the reduced frequency. The increase in the oscillation angle increases the upper and lower limits of the lift, and the "∞" shape of the lift curve is more obvious. The intersection position of the lift hysteresis curve is proportional to the oscillation angle of attack and inversely proportional to the reduced frequency. The maximum increase in lift can reach 46.15% under the condition. Once the surface pressure of the blade exceeds the rated value, the blade may have a rupture under such conditions in a long time.
3. In one cycle that the airfoil is from upward to down, as the angle of attack increases, the trailing edge vortex appears along with the flow separation, and the trailing edge vortex moves to the front edge to expand the range of the vortex. Once the rolled shear layer is unstable, it will cause the large eddy to split into small eddy. As the downward angle of the blade decreases, the trailing edge vortex gradually disappears. The generation, expansion, splitting and detachment of the vortex in one cycle are the main reasons for the change of lift. The same angle of attack could correspond to two different lift values. The distribution of lift coefficient exhibits hysteresis characteristics, which is completely different from the static angle change, and is unique to the dynamic stall of the blade.

Acknowledgements This research was financially supported by National Natural Science Foundation of China (Grant Nos. 51705002, 51505003), the Natural Science Foundation of Anhui Province of China (Grant Nos. 1708085QE123 and 1708085QA17) and Young Teachers Fund for Scientific Research of Anhui University of Science and Technology (Grant No. QN2018106).

References

1. Z. Shanyuan, A new type of energy resources in 21st century-wind Energy. Jiangxi Energy **1**(37–38), 35 (2001). **(in Chinese)**

2. M.V. Ol, L. Bernal, C.K. Kang et al., Shallow and deep dynamic stall for flapping low Reynolds number airfoils. Exp. Fluids **46**(5), 883–901 (2009)
3. W. Shyy, H. Aono, S.K. Chimakurthi et al., Recent progress in flapping wing aerodynamics and aeroelasticity. Prog. Aerosp. Sci. **46**(7), 284–327 (2010)
4. J.G. Leishman, Challenges in modeling the unsteady aerodynamics of wind turbines. Wind Energy **5**(2–3), 85–132 (2002)
5. W.J. McCroskey, L.W. Carr, K.W. McAlister, Dynamic stall experiments on oscillating airfoils. AIAA J. **14**(1), 57–63 (1976)
6. D. Simms, S. Schreck, M. Hand et al., *NREL Unsteady Aerodynamics Experiment in the NASA-Ames Wind Tunnel: A Comparison of Predictions to Measurements* (Office of Scientific & Technical Information Technical Reports, 2001)
7. W. Long, L.I. Liang, S. Lun-ye et al., Effect of jet parameters on the aerodynamic performance for the wind turbine blade. Fluid Mach. **45**(7), 28–33 (2017). **(in Chinese)**
8. W. Long, S. Lunye, Z. Jin, Study of the impact of the change of slotted position at high angle of attack on wind turbine blades. J. Hefei Univ. Technol. (Natural Science) **40**(8), 1037–1041 (2017). **(in Chinese)**
9. P. Gerontakos, T. Lee, Near wake behind an airfoil with leading-edge flow control. J. Aircr. **42**(2), 561–568 (2015)
10. P. Gerontakos, T. Lee, Active trailing-edge flap control of oscillating-wing tip vortex. Aiaa J. **44**(11), 2746–2754 (2006)
11. S.L. Yang, Y.L. Chang, O. Arici, Incompressible Navier-Stokes computation of the NREL airfoils using a symmetric total variational diminishing scheme. J. Sol. Energy Eng. **116**(4), 174–182 (1994)
12. Y. Kim, Z.T. Xie, Modelling the effect of freestream turbulence on dynamic stall of wind turbine blades. Comput. Fluids **129**, 53–66 (2016)
13. J. Yen, N.A. Ahmed, Enhancing vertical axis wind turbine by dynamic stall control using synthetic jets. J. Wind Eng. Ind. Aerodyn. **114**(114), 12–17 (2013)
14. S. Gupta, J.G. Leishman, Dynamic stall modeling of the S809 aerofoil and comparison with experiments. Wind Energy **9**(6), 521–547 (2006)
15. L. Peng-yin, C. Jin-ge, Z. Xiao-cheng et al., Reduced-order models for unsteady aerodynamic load of wind turbines. J. Eng. Thermophys. **36**(10), 2165–2168 (2015). **(in Chinese)**
16. S. Mao, W. Jia-lu, L. Qix-iang, A study of the flow structure around a constant-rate pitching airfoil. Acta Mech. Sin. **24**(5), 517–521 (1992). **(in Chinese)**
17. B. Peng, C. Erjie, Z. Weijiang et al., Investigation of the dynamic stall about the pitching airfoil. Acta. Mech. Sin. **36**(5), 569–576 (2004). **(in Chinese)**
18. A. Choudhry, R. Leknys, M. Arjomandi et al., An insight into the dynamic stall lift characteristics. Exp. Therm. Fluid Sci. **58**(4), 188–208 (2014)
19. J.G. Holierhoek, J.B. Vaal, A.H.V. Zuijlen et al., Comparing different dynamic stall models. Wind Energy **16**(1), 139–158 (2013)
20. H.K. Versteeg, W. Malalasekera, *An Introduction to Computational Fluid Dynamics—The Finite Method* (World Book Publishing Company, Cleveland, 1995)
21. E. Duque, M. Burkland, W. Johnson, Navier-Stokes and comprehensive analysis performance predictions of the NREL phase VI experiment. J. Sol. Energy Eng. **125**(4), 43–61 (2006)
22. A.J. Chorin, Numerical solution of the Navier-Stokes equations. Math. Comput. **22**(104), 17–34 (1989)
23. P. Spalart, S. Allmaras, A one-equation turbulence model for aerodynamic flows. Recherche Aerospatiale **1**(1), 5–21 (1994)
24. U. Piomelli, Wall-layer models for large-eddy simulations. Prog. Aerosp. Sci. **44**(6), 437–446 (2008)
25. D.D. Apsley, M.A. Leschziner, Advanced turbulence modelling of separated flow in a diffuser. Flow Turbul. Combust. **63**(1–4), 81–112 (2000)
26. L. Wang, L.Y. Sun, G. Wu et al., *Research on algorithm of blade vibration for general wind turbine*. International Symposium on Precision Mechanical Measurements (International Society for Optics and Photonics, 2016), p. 990325
27. P. Knupp, L.G. Margolin, M. Shashkov, Reference Jacobian optimization-based rezone strategies for arbitrary Lagrangian Eulerian methods. J. Comput. Phys. **176**(1), 93–128 (2002)
28. S.H. Huo, F.S. Wang, W.Z. Yan et al., Review: layered elastic solid method for the generation of unstructured dynamic mesh. Finite Elem. Anal. Des. **46**(10), 949–955 (2010)
29. H. Jeffrey, J. Shi, An all-speed asymptotic-preserving method for the isentropic Euler and Navier-Stokes equations. Commun. Comput. Phys. **12**(4), 955–980 (2012)
30. G. Lalor, A. Mullane, M. O'Malley, Frequency control and wind turbine technologies. IEEE Trans. Power Syst. **20**(4), 1905–1913 (2005)
31. G.R. Srinivasan, W.J. Mccroskey, Navier-Stokes calculations of hovering rotor flow fields. J. Aircr. **25**(10), 865–874 (1988)
32. R.F. Ramsay, M.J. Hoffman, G.M. Gregorek, *Effects of grit roughness and pitch oscillation on the S809 airfoil. NREL/TP-442-7817* (Office of Scientific & Technical Information Technical Reports, 1995)

Publisher's Note Springer Nature remains neutral with regard to jurisdictional claims in published maps and institutional affiliations.